

1 **Original Article**

2  
3  
4 **MRI Cross Sectional Atlas of Normal Canine Cervical Musculoskeletal Structure**

5  
6  
7 M. Alizadeh <sup>a, \*</sup>, C. Zindl <sup>b, \*\*</sup>, M.J. Allen <sup>b</sup>, G.G. Knapik <sup>a</sup>, N. Fitzpatrick <sup>c</sup>, W.S. Marras <sup>a</sup>

8  
9 <sup>a</sup> *Spine research Institute, The Ohio State University, 520 Baker Systems, 1971 Neil Avenue.,*  
10 *Columbus, Ohio 43210 USA*

11 <sup>b</sup> *Surgical Discovery Center, Department of Veterinary Medicine, University of Cambridge,*  
12 *Madingley Road, Cambridge, CB3 0ES, UK*

13 <sup>c</sup> *Fitzpatrick Referrals, Eashing, Surrey GU7 2QQ, UK*  
14  
15  
16  
17  
18  
19

20 \* Corresponding author. Tel.: +16787722108

21  
22 *E-mail address:* alizadeh.3@osu.edu (Name: Mina Alizadeh).

23 *Full postal address: The Ohio State University, Spine Research Institute, 1971 Neil Avenue*

24 *Room 520, Columbus, OH, USA. 43210.*

25 \*\* *Equally contributed to the work*  
26

## Abstract

Although magnetic resonance imaging (MRI) has been increasingly used as a diagnostic tool for cervical spine injuries in canines, a comprehensive normal MRI anatomy of the canine cervical spine muscles is lacking. Therefore, the purpose of this study was to build a magnetic resonance imaging atlas of the normal cross sectional anatomy of the muscles of the canine cervical spine. MRI scans were performed on a canine cadaver using a combination of T1 and T2-weighted images in the transverse, sagittal and dorsal planes acquired at a slice thickness of 1 mm. Muscle contours were traced manually in each slice, using local osseous structures as reference points for muscle identification. Twenty-two muscles were traced in 401 slices in the cervical region. A three dimensional surface model of all the contoured muscles was created to illustrate the complex geometrical arrangement of canine neck muscles. The cross-sectional area of the muscles was measured at the mid-level of each vertebra. The accuracy of the location of the mapped muscles was verified by comparing the sagittal view of the 3D model of muscles with still photographs obtained from anatomic canine cadaver dissection. We believe this information will provide a unique and valuable resource for veterinary researchers, clinicians and surgeons who wish to evaluate MRI images of the cervical spine. It will also serve as the foundation for ongoing work to develop a computational model of the canine cervical spine in which anatomical information is combined with electromyographic, kinematic and kinetic data.

*Keywords:* dog; neck; cross sectional anatomy; magnetic resonance imaging

## 1. Introduction

Biomechanical cervical spine models have been used extensively to evaluate feasibility and potential side effects of surgical procedures and instrumentation as it is currently not feasible to directly measure spinal loading in-vivo (Jaeger et al., 2011). Theoretical and numerical biomechanical models of the human cervical spine have been developed over the last three decades to investigate kinetics and kinematics of the neck (Dugailly et al., 2011). However, these models have not been translated to the canine cervical spine in spite of the high incidence of spinal disorders and injuries (Jeffery et al., 2013). Successful development and implementation of these models in canine spinal studies would require accurate anatomical data of the underlying soft tissues and bone (Sharir et al., 2006). Among the many components which should be incorporated into a model, muscles play a vital role in stability, loading and locomotion as they exert the majority of the required moments to maintain equilibrium in different postures and to perform various tasks (Nussbaum et al., 1995; Vasavada et al., 1998). Studies have shown the substantial effect of muscle forces on cervical spine kinematics and injury potential on the neck structure (Borst et al., 2011). To this extent, comprehensive knowledge of canine muscle properties including estimation of muscle forces and orientation has yet to be established.

The magnitude of the maximum muscle force generation potential in part depends on the muscle morphometric parameters such as physiological cross-sectional area, muscle fiber direction along the length of the muscle, and the muscle attachment site among many other factors (Marras et al., 2001). Therefore, in order to develop an accurate canine specific cervical model, the muscle cross-sectional area (CSA) needs to be directly measured and incorporated.

These geometric properties are usually obtained from anatomic atlases, cadaveric studies or medical images such as computed tomography (CT) and magnetic resonance imaging (MRI). Regardless of technique, regional cross-sectional anatomy is of great importance in identifying the muscle of interest and to determine its biomechanical properties (Zotti et al., 2009). MRI has been used increasingly in dogs as a diagnostic technique for musculoskeletal injuries, joint diseases and soft tissue tumors. It also had become the preferred imaging modality for investigating articular cartilage, meniscus and ligaments since it provides excellent visualization of soft tissue (Soler et al., 2007; Van Caelenberg et al., 2011; Zook et al., 1989). However a comprehensive search of the literature showed that normal MRI cross-sectional anatomy of the canine neck muscles does not exist. George and Smallwood 1992, had provided an atlas for head and neck using CT in the mesaticephalic dogs. Nevertheless, due to the inability of CT images to differentiate between muscles it is not a comprehensive regional atlas for muscular structure of the canine neck. Hence, the primary aim of this study was to 1) build a comprehensive atlas of cross-sectional anatomy of canine cervical spine muscles using MRI datasets and 2) measure individual CSA of canine cervical spine muscles at each cervical level. This would help to provide a suitable platform for the potential development of a canine specific dynamic biomechanical model of the neck.

We believe that significant insights can be gained from MRI slice base representations. This information will help researchers and clinicians to better evaluate MRI images and enable them to precisely identify and visualize muscular structures of their interest. This project will also be useful for surgeons during pre-operative planning helping identify musculoskeletal structures in the canine neck area. Therefore the purpose of this study was first to provide a cross-sectional anatomy atlas of the canine cervical spine muscles by tracing them with different colors. Second, documenting major force producing neck muscles CSA

## 2. Materials and methods

### 2.1 Specimen

A skeletally mature male hound dog (26.0 kg body weight) that was euthanized for reasons unrelated to this study served as the subject. The dog was healthy, with no evidence of joint or spinal disease. It was housed in a single kennel in a room together with other dogs and was fed a standard laboratory dog chow diet with water *ad libitum*. The experimental procedures for this study were reviewed and approved by the local institutional animal care and use committee (IACUC).

### 2.2 MRI imaging

T1 and T2 weighted MRI images were acquired on a 3T MRI scanner (Magnetom Trio, Siemens Healthcare, Erlangen, Germany). Transverse slices of 1 mm thickness were obtained from the skull level and extended caudally to the level of the second thoracic vertebra. MRI examination was performed less than 1 hour after euthanasia to reduce dehydration effects on muscles as much as possible. An MRI-compatible jig was designed to aid in positioning the dog inside the MRI machine. The dog was positioned in ventral recumbency with the thoracic limbs placed in an extended position next to the cervical area and the neck kept in a fairly neutral posture by supporting the neck area with a pillow (Fig.1).

### 2.3 Image analysis

The files generated in DICOM format were retrieved and analyzed with Mimics® software (Materialise NV Technologielaan 15, 3001 Leuven, Belgium). T1-weighted images of all slices from the occiput to the first thoracic vertebra were analyzed. To begin with, bony

structures and muscles were differentiated with the thresholding and region growing applications of the imaging program. Only left sided muscles were traced since it was assumed that spinal musculature would be symmetric. Muscles were traced in each slice based on the visible bony landmarks and the aid of literature about canine anatomy (Boyd et al., 2001; Budras et al., 2007; Kumar, 2012; Miller and Christensen, 1964; Nickel et al., 1992). Each muscle was assigned a separate mask to enhance visualization for outlining of muscle borders and following CSA measurements (Fig 2-8). CSA of the traced muscles were measured at the mid-level of each vertebra (Marras et al., 2001).

## 2.4 Validation

The relative locations of the different neck muscles were compared to photographic images obtained during anatomic canine cadaver dissection. During dissection, the neck muscles were visually identified and separated by removing connective tissues while preserving each muscle's origin and insertion. Following the separation of the muscles, photographs were obtained at different stages of the dissection to compare them with the generated 3D models of the mapped muscles (Fig 9-11).

## 3. Results

### 3.1 Canine cervical muscles mapped from MRI

Twenty-two canine cervical spine muscles were traced and labeled on 441 transverse MRI image slices (Fig 2-8). Only those muscles that play a role in movement of the neck and partly in the head were considered and grouped as follows: 1. superficial and deep muscle layers of the shoulder girdle; 2. long (superficial, medial, intermediate, deep layers) and short muscles, representing extensors, rotators and neck lateral bending muscles; 3. neck flexors; 4. movers of the head (Nickel et al., 1992; Schomacher and Falla, 2013).

From the superficial shoulder girdle muscle group, the M.trapezius cervicis, M.omotransversarius, M.sternocephalicus, M.cleidomastoideus and M.cleidocervicalis as parts of the M.brachiocephalicus; from the deep shoulder girdle muscle group, the M.rhomboideus and M.serratus ventralis were included. The long neck muscles were represented by the M.splenius as the superficial layer, the M.longissimus (capitis and cervicis), M.longissimus thoracis and M.iliocostalis thoracis as part of the medium layer and the M.spinalis et semispinalis cervicis, M.semispinalis capitis (biventer and complexus) and M.multifidus cervicis as the deep layer. The short neck muscles were represented by the M.intertransversarii cervicis only. On the ventral neck area, the M.longus colli and M.scalenus were traced as the neck flexors. Included muscles that are considered movers of the head were the M.longus capitis, M. rectus capitis dorsalis major, the M.obliquus capitis (caudalis and cranialis) and the M.rectus capitis lateralis and M.rectus capitis ventralis. The M.cleidobrachialis, M.interspinal cervicis, and the M.rectus capitis dorsalis minor were not traced. A three dimensional (3D) model of all the identified and contoured muscles was created to illustrate neck muscle location in 3D (Fig 8-9).

### *3.2 Cross-sectional area of canine cervical muscles*

The CSA were measured in all 22 canine cervical muscles that were discriminated in MRI images and results are shown in Table 1. Based on the length of the muscles, in this study, they were grouped in three categories - long, medium and short muscles. The long muscles are defined as extending either over the whole neck area, from C1-C2 into the thoracic area. This group includes the M.rhomboideus, M.splenius, M.semispinalis capitis (biventer and complexus), and M.longissimus capitis. Or they are defined as extending over six vertebrae, with additional segmental insertions / origins such as the M.longus capitis, M.longus colli, M.intertransversarii cervicis. Medium muscles are defined as extending over either five

vertebrae such as the M.cleidocervicalis, M.sternocephalicus, M.cleidomastoideus, M.omotransversarius, M.trapezius cervicis, M.spinalis et semispinalis cervicis, M.multifidus cervicis and M.longissimus cervicis or over four vertebrae including the M.serratus ventralis and M.scalenus. Short muscles are defined as those presented at only one level such as the M.obliquus capitis cranialis, M.rectus capitis lateralis and M.rectus capitis ventralis or two levels including M.obliquus capitis caudalis and M.rectus capitis dorsalis major.

#### **4. Discussion**

This study is part of an effort to develop a biologically-assisted musculoskeletal canine cervical spine biomechanical model. Biomechanical models can be of great value in identifying potential pathways for neck disorders. They represent a quantitative method to evaluate mechanical effects of surgical techniques and interbody implants on spine. This research provides fundamental information for the initial development of a canine cervical spine model. However, in order to generalize the outcome of this study, more studies will be necessary that involve more specimens. None the less, this study provides a platform for future investigations. This study, for the first time, has implemented a well-developed precise human biomechanical approach to quantify cervical spine muscle CSA (as opposed to cadaveric studies which have several disadvantages).

In the present study we characterized the anatomical trajectory of the majority of the canine cervical muscles with magnetic resonance imaging in a visual way to build an MRI based cross-sectional atlas of the canine cervical spine muscles. Major force producing muscles of the canine cervical spine were identified by measuring the cross-sectional area of individual muscles.

MRI is a noninvasive cross-sectional imaging technique appropriate for diagnostic, research and teaching purposes (Anastasi et al., 2007) with many advantages compared to



other medical imaging techniques (Alsafy, 2008). Soft tissues such as muscles are not readily observed with other radiological modalities in a way that the borders between different muscles can be distinguished. MRI provides excellent detail of clinically relevant anatomy (Soler et al., 2007). Considering MRI spatial resolution, this imaging technique is more sensitive in discriminating different soft tissues, detecting diseases and distinguishing normal and abnormal structures and has been widely used in dogs in musculoskeletal imaging (Adamiak et al., 2011; Agnello et al., 2008; De Bakker et al., 2014; Schaefer and Forrest, 2006) . However, accurate interpretation and identification of CT and MRI images require comprehensive knowledge of the normal planimetric anatomy of the muscles in the region of interest (Rivero et al., 2005).

This study denotes the musculoskeletal cross-sectional anatomy of the canine cervical spine from the occiput to the first thoracic vertebra. Muscles on MRI images were identified and classified with the help of several anatomy books describing the origin, trajectory and insertion of the muscles in text and drawings ( Miller and Christensen, 1964; Nickel et al., 1992) together with photographs of cross-sectional reference cuts (Boyd et al., 2001; Kumar, 2012). The anatomic detail of some muscles showed slight discrepancy especially regarding the photographs of the reference cuts, which was probably due to breed differences, as Boyd et al (2001) used a Beagle for his study compared to the hound used in our study. This made the differentiation and identification of muscles sometimes challenging.

Muscles with several portions were treated as a single muscle body regardless of their different divisions as it was challenging to separate muscles into their distinguished bundles. For instance, the M.intertransversarii cervicis anatomically consisting of the M.intertransversarii dorsalis cervicis, the M.intertransversarii intermedii cervicis and the M.intertransversarii ventralis cervicis, was considered as one single muscle body.

The ability to use all three imaging planes (sagittal, dorsal and transverse) at the same time on one screen in the Mimics® software, made it easier to interactively distinguish and mark the individual muscles. The 3D view substantially aided in the identification of muscles in their complex geometrical arrangement as was described in an earlier study (Jaeger et al., 2011).

The main purpose of this investigation was to map the major muscular actuators of cervical motion. The emphasis was on defining the bulk of the muscle mass, since the origins and insertions have been well established before; for this reason, the muscle bundles were not separated into bundles and no attempt was made to map serrations. We mainly focused on muscles that have major contributions to either moving or stabilizing the neck, regardless of their role in shoulder or limb movements. Twenty-two muscles were identified and mapped, the majority of those do play an active role in movement on the neck and head. We also included some muscles of the shoulder girdle that participate in neck movement (M.sternocephalicus, M.brachiocephalicus, M.rhomboideus and M.serratus ventralis). The M.cleidobrachialis part of the M.brachiocephalicus was not mapped as its insertion on the humerus was not in the field of view of the MR images – the same was true for the M.pectoralis (superficialis and profundus). The M.platysma was not mapped because this muscle was very difficult to identify on MR images due to its flat appearance and origin and insertion points mainly emerging out of aponeuroses. We were not able to identify two of the short neck muscles M.interspinal cervicis and the M.rectus capitis dorsalis minor with confidence. These muscle bellies are small and either span a very short distance between adjacent vertebrae or, in case of the M. rectus capitis dorsalis minor, become merged with the M. rectus capitis dorsalis major. Furthermore, although muscles of the deep layer, such as the M.intertransversarii cervicis were mapped, it was challenging and we were not able to trace them precisely.

Several sequences are reported for use in MRI diagnostic imaging. The T1-weighted images used in the present study to identify the individual muscles, have been reported to give good anatomical detail to identify musculoskeletal structures (Agnello et al., 2008; Baeumlin et al., 2010; Soler et al., 2007; Van Caelenberg et al., 2011). However, it was difficult to map smaller muscles (M.interspinal cervicis and M. rectus capitis dorsalis minor). The muscle size, unclear connective tissue borders between those muscles, and the inability to visually separate muscles due to resolution factors of the 3T MRI machine are the factors that contributed to prevent us from mapping those smaller muscles. The small voxel size of a 3T MRI scanner gives a higher resolution. However, it leads to a much lower signal-to-noise ratio which reduces the ability to identify small structures (Sunico et al., 2012). The same study found that imaging the same specimen with a proton density sequence maximizes the distinction of muscular borders compared to T1 or T2 sequences (Sunico et al., 2012).

In general the CSA measurements are not in agreement with the report by Sharir et al. (2006). This conflict potentially might be due to several reasons, most probably as muscle mass might be different between dogs of different breeds and also between individual dogs. Muscle morphometric measurements were taken after dissection of the muscle in Sharir et al (2006). Disturbing muscle connections with the surrounding connective tissue may affect its anatomical properties such as its length and width, which might have influenced measurements of the muscle cross section area. Different approaches were taken to present muscle CSA, which increases the possibility of incompatibility between measurements. Sharir et al., (2006) represented the physiological CSA of an individual muscle as a ratio of muscle volume to its effective fascicle length while in the present study we measured actual CSA for each muscle at different levels on MRI images. Therefore, in the study obtained by Sharir et al., (2006), constant cross section throughout the length of the muscles was assumed.

Although this assumption might be valid for small muscles in the neck region, it is not an appropriate representation for fan shaped muscles that have various attachments, as most of the neck muscles present anatomically. These variations within the reported literature highlight the need for quantitative assessments using up to date technological approaches.

The present study has several limitations. Only a single subject was evaluated, due to the nature of this study being exploratory research. The ventral recumbency position of the dog on the MRI table with the thoracic limbs positioned next to the cervical area with flexed shoulder and elbow joints, might have resulted in altered muscle location and orientation in comparison to a neutral standing position, with extended shoulder and elbow joints. By positioning a pillow underneath the neck area, we tried to keep the neck posture as close as possible to a posture in a standing position, however extended shoulder and elbow joints could not be completely replicated. In spite of the excellent capability of MR images in differentiating between muscles, it was still difficult to distinguish all muscles in the region of interest, especially muscles of the deep layer. Therefore, we primarily aimed to identify muscles in the superficial and medium layer of the neck region, as they are the main actuators in stabilizing and moving the neck. With concurrent computed tomography imaging and evaluation of photographic images of cross-sectional frozen cuts of the same individual, it might have been possible to develop more accurate information to identify the muscles of the deep layer on MR images, but this was beyond of the financial possibilities of this study.

While it is clear that there is likely to be significant breed-to-breed variation particularly in muscle mass, we believe that the data presented in this study can be implemented to develop a canine specific cervical biomechanical model as well as to be used as a guide for future medical imaging investigations such as muscle bilateral symmetry assumption.

## **Conclusions**

The data from this work has allowed for the production of the first comprehensive multi-segmental MRI atlas on the cross-sectional anatomy of the canine cervical spine musculature. We anticipate that the 2D and 3D images from this work will be useful to clinicians and researchers working with the canine cervical spine. They will also serve as the foundation of a more expansive project to combine anatomical and EMG data to produce a computational biomechanical model of the canine cervical spine that can be used to study the impact of both pathology and surgical treatment on spinal kinetics and kinematics.

## **Conflict of interest statement**

None declared.

## **Acknowledgements**

This work was supported in part by Fitzpatrick Referrals Ltd., through the One Health/One Medicine Fellowship at The Ohio State University.

## 319 References

- 320 Adamiak, Z., Jaskólska, M., Matyjasik, H., Pomianowski, A., Kwiatkowska, M., 2011.  
321 Magnetic resonance imaging of selected limb joints in dogs. *Pol. J. Vet. Sci.* 14, 501–  
322 505.
- 323 Agnello, K.A., Puchalski, S.M., Wisner, E.R., Schulz, K.S., Kapatkin, A.S., 2008. Effect of  
324 Positioning, Scan Plane, and Arthrography on Visibility of Periarticular Canine  
325 Shoulder Soft Tissue Structures on Magnetic Resonance Images. *Vet. Radiol.*  
326 *Ultrasound* 49, 529–539. doi:10.1111/j.1740-8261.2008.00429.x
- 327 Alsafy, M.A.M., 2008. Computed tomography and cross-sectional anatomy of the thorax of  
328 goat. *Small Rumin. Res.* 79, 158–166. doi:10.1016/j.smallrumres.2008.07.028
- 329 Anastasi, G., Bramanti, P., Di Bella, P., Favalaro, A., Trimarchi, F., Magaudo, L., Gaeta, M.,  
330 Scribano, E., Bruschetta, D., Milardi, D., 2007. Volume rendering based on magnetic  
331 resonance imaging: advances in understanding the three-dimensional anatomy of the  
332 human knee. *J. Anat.* 211, 399–406. doi:10.1111/j.1469-7580.2007.00770.x
- 333 Baeumlin, Y., De Rycke, L., Van Caelenberg, A., Van Bree, H., Gielen, I., 2010. Magnetic  
334 resonance imaging of the canine elbow: an anatomic study. *Vet. Surg.* VS 39, 566–  
335 573. doi:10.1111/j.1532-950X.2010.00690.x
- 336 Borst, J., Forbes, P.A., Happee, R., Veeger, D. (H. E.J.), 2011. Muscle parameters for  
337 musculoskeletal modelling of the human neck. *Clin. Biomech.* 26, 343–351.  
338 doi:10.1016/j.clinbiomech.2010.11.019
- 339 Boyd, J.S., Paterson, C., May, A.H., 2001. *Clinical anatomy of the dog & cat.* Harcourt  
340 Publishers Limited, Jamestown Road, London.
- 341 Budras, K.D., McCarthy, P.H., Fricke, W., Richter, R., Horowitz, A., Berg, R., 2007.  
342 *Anatomy of the Dog: An Illustrated Text, Fifth Edition.* Schluetersche, Germany.
- 343 De Bakker, E., Gielen, I., Kromhout, K., van Bree, H., Van Ryssen, B., 2014. Magnetic  
344 resonance imaging of primary and concomitant flexor enthesopathy in the canine  
345 elbow. *Vet. Radiol. Ultrasound Off. J. Am. Coll. Vet. Radiol. Int. Vet. Radiol. Assoc.*  
346 55, 56–62. doi:10.1111/vru.12090
- 347 Dugailly, P.-M., Sobczak, S., Moiseev, F., Sholukha, V., Salvia, P., Feipel, V., Rooze, M.,  
348 Van Sint Jan, S., 2011. Musculoskeletal modeling of the suboccipital spine:  
349 kinematics analysis, muscle lengths, and muscle moment arms during axial rotation  
350 and flexion extension. *Spine* 36, E413–422. doi:10.1097/BRS.0b013e3181dc844a
- 351 Evans, H.E., Lahunta, A. de, 2013. *Miller's Anatomy of the Dog*, 4th ed. Saunders.
- 352 George, T.F., Smallwood, J.E., 1992. *Anatomic Atlas for Computed Tomography in the*  
353 *Mesaticephalic Dog: Head and Neck.* *Vet. Radiol. Ultrasound* 33, 217–240.  
354 doi:10.1111/j.1740-8261.1992.tb00136.x
- 355 Jaeger, R., Mauch, F., Markert, B., 2011. The muscle line of action in current models of the  
356 human cervical spine: a comparison with in vivo MRI data. *Comput. Methods*  
357 *Biomech. Biomed. Engin.* 15, 953–961. doi:10.1080/10255842.2011.567982
- 358 Jeffery, N. d., Levine, J. m., Olby, N. j., Stein, V. m., 2013. Intervertebral Disk Degeneration  
359 in Dogs: Consequences, Diagnosis, Treatment, and Future Directions. *J. Vet. Intern.*  
360 *Med.* 27, 1318–1333. doi:10.1111/jvim.12183
- 361 Kumar, M.S.A., 2012. *Clinically Oriented Anatomy of the Dog and Cat.* Linus Publications,  
362 Ronkonkoma, NY 11779.
- 363 Marras, W.S., Jorgensen, M.J., Granata, K.P., Wiand, B., 2001. Female and male trunk  
364 geometry: size and prediction of the spine loading trunk muscles derived from MRI.  
365 *Clin. Biomech.* Bristol Avon 16, 38–46.
- 366 Miller, M.E., Christensen, G. c., 1964. *Anatomy of the Dog*, 4th ed. Saunders company,  
367 philadelphia.

- Nickel, R., Schummer, A., Seiferle, E., 1992. Lehrbuch der Anatomie der Haustiere, 6th ed. Paul Parey, Berlin and Hamburg, Germany.
- Nussbaum, M.A., Chaffin, D.B., Rechten, C.J., 1995. Muscle lines-of-action affect predicted forces in optimization-based spine muscle modeling. *J. Biomech.* 28, 401–409.
- Rivero, M.A., Ramírez, J.A., Vázquez, J.M., Gil, F., Ramírez, G., Arencibia, A., 2005. Normal anatomical imaging of the thorax in three dogs: computed tomography and macroscopic cross sections with vascular injection. *Anat. Histol. Embryol.* 34, 215–219. doi:10.1111/j.1439-0264.2005.00596.x
- Schaefer, S.L., Forrest, L.J., 2006. Magnetic Resonance Imaging of the Canine Shoulder: An Anatomic Study. *Vet. Surg.* 35, 721–728. doi:10.1111/j.1532-950X.2006.00216.x
- Schomacher, J., Falla, D., 2013. Function and structure of the deep cervical extensor muscles in patients with neck pain. *Man. Ther.* 18, 360–366. doi:10.1016/j.math.2013.05.009
- Sharir, A., Milgram, J., Shahar, R., 2006. Structural and functional anatomy of the neck musculature of the dog (*Canis familiaris*). *J. Anat.* 208, 331–351. doi:10.1111/j.1469-7580.2006.00533.x
- Soler, M., Murciano, J., Latorre, R., Belda, E., Rodríguez, M.J., Agut, A., 2007. Ultrasonographic, computed tomographic and magnetic resonance imaging anatomy of the normal canine stifle joint. *Vet. J.* 174, 351–361. doi:10.1016/j.tvjl.2006.08.019
- Sunico, S.K., Hamel, C., Styner, M., Robertson, I.D., Kornegay, J.N., Bettini, C., Parks, J., Wilber, K., Smallwood, J.E., Thrall, D.E., 2012. Two anatomic resources of canine pelvic limb muscles based on CT and MRI. *Vet. Radiol. Ultrasound Off. J. Am. Coll. Vet. Radiol. Int. Vet. Radiol. Assoc.* 53, 266–272. doi:10.1111/j.1740-8261.2012.01926.x
- Van Caelenberg, A.I., De Rycke, L.M., Hermans, K., Verhaert, L., van Bree, H.J., Gielen, I.M., 2011. Low-field magnetic resonance imaging and cross-sectional anatomy of the rabbit head. *Vet. J. Lond. Engl.* 188, 83–91. doi:10.1016/j.tvjl.2010.02.020
- Vasavada, A.N., Li, S., Delp, S.L., 1998. Influence of muscle morphometry and moment arms on the moment-generating capacity of human neck muscles. *Spine* 23, 412–422.
- Zook, B.C., Hitzelberg, R.A., Bradley, E.W., 1989. Cross-Sectional Anatomy of the Beagle Thorax. *Vet. Radiol.* 30, 277–281. doi:10.1111/j.1740-8261.1989.tb01800.x
- Zotti, A., Banzato, T., Cozzi, B., 2009. Cross-sectional anatomy of the rabbit neck and trunk: comparison of computed tomography and cadaver anatomy. *Res. Vet. Sci.* 87, 171–176. doi:10.1016/j.rvsc.2009.02.003

## Figure legends

Fig.1. MRI of the occipital, cervical and cervico-thoracic area in the sagittal plane. Vertical lines indicate the MRI slice corresponding to the presented images (Fig 2-8). The more cranial slice represents section (a) and the more caudal slice represents section (b) of Figures 2-8.

Fig.2. T1-weighted MRI image at (C1). (a) Cranial C1. (b) Mid-vertebral C1. Muscles are listed dorsal to ventral, left to right.

□ C1 and C2

■ M.cleidocervicalis

■ M.rhomboideus

■ M.splenius

■ M.cleidomastoideus

■ M.semispinalis capitis (Biventer)

■ M.semispinalis capitis (Complexus)

■ M.longissimus capitis

■ M.sternocephalicus

■ M. rectus capitis dorsalis major

■ M.obliquus capitis caudalis

■ M.obliquus capitis cranialis

■ M.rectus capitis lateralis


■ M. rectus capitis ventralis

■ M.longus capitis

■ M.longus colli




436 Fig.3. T1-weighted MRI image at (C2). (a) Cranial C2. (b) Mid-vertebral C2. Muscles are  
437 listed dorsal to ventral, left to right.


438  Wing of Atlas (C1) and C2

439  M.cleidocervicalis


440  M.rhomboideus


441  M.splenius


442  M.cleidomastoideus


443  M.semispinalis capitis (Biventer)


444  M.semispinalis capitis (Complexus)


445  M.longissimus capitis


446  M.rectus capitis lateralis

447  M.omotransversarius

448  M.rectus capitis dorsalis major

449  M.obliquus capitis caudalis

450  M.sternocephalicus

451  M.rectus capitis ventralis

452  M.intertransversarii cervicis

453  M.longus capitis

454  M.longus colli

455

456





















457

458

459

460

461 Fig.4. T1-weighted MRI image at (C3). (a) Cranial C3. (b) Mid-vertebral C3. Muscles are  
462 listed dorsal to ventral, left to right.

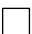
- 463  C3 and articular process of C4
- 464  M.trapezius cervicis
- 465  M.cleidocervicalis
- 466  M.rhomboideus
- 467  M.splenius
- 468  M.serratus ventralis
- 469  M.omotransversarius
- 470  M.cleidomastoideus
- 471  M.semispinalis capitis (Biventer)
- 472  M.semispinalis capitis (Complexus)
- 473  M.longissimus capitis
- 474  M.longissimus cervicis
- 475  M.intertransversarii cervicis
- 476  M.scalenus
- 477  M.longus capitis
- 478  M.sternocephalicus
- 479  Nuchal ligament
- 480  M.spinalis et semispinalis cervicis
- 481  M.multifidus cervicis
- 482  M.longus colli

483

484

485

486 Fig.5. T1-weighted MRI image at (C4). (a) Cranial C4. (b) Mid-vertebral C4. Muscles are  
487 listed dorsal to ventral, left to right.

488  C4 (a, b) and tuberculum ventrale of transverse process of C3 (a)

489  M.trapezius cervicis

490  M.cleidocervicalis

491  M.rhomboideus


492  M.splenius


493  M.serratus ventralis


494  M.omotransversarius

495  M.cleidomastoideus

496  M.semispinalis capitis (Biventer)

497  M.semispinalis capitis (Complexus)

498  M.longissimus capitis

499  M.longissimus cervicis


500  M.intertransversarii cervicis


501  M.scalenus

502  M.longus capitis

503  M.sternocephalicus

504  Nuchal ligament

505  M.spinalis et semispinalis cervicis


506  M.multifidus cervicis

507  M.longus colli

508

509


510 Fig.6. T1-weighted MRI image at (C5). (a) Cranial C5. (b) Mid-vertebral C5. Muscles are  
511 listed dorsal to ventral, Left to Right.

512  C4 articular process and C5

513  M.trapezius cervicis

514  M.rhomboideus

515  M.splenius

516  M.serratus ventralis


517  M.cleidocervicalis

518  M.omotransversarius

519  M.semispinalis capitis (Biventer)

520  M.semispinalis capitis (Complexus)

521  M.longissimus capitis


522  M.longissimus cervicis

523  M.intertransversarii cervicis


524  M.scalenus


525  M.longus capitis

526  M.cleidomastoideus

527  M.sternocephalicus

528  Nuchal ligament

529  M.spinalis et semispinalis cervicis

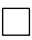
530  M.multifidus cervicis

531  M.longus colli


532

533

534 Fig.7. T1-weighted MRI image at (C6). (a) Cranial C6. (b) Mid-vertebral C6. Muscles are  
535 listed dorsal to ventral, left to right.

536  C6

537  Articulatio humeri (a) and Scapula (b)

538  M.trapezius cervicis

539  M.omotransversarius

540  M.rhomboideus


541  M.splenius

542  M.serratus ventralis

543  M.semispinalis capitis (Biventer)

544  M.semispinalis capitis (Complexus)


545  M.longissimus capitis


546  M.longissimus cervicis

547  M.longissimus thoracis and M.illiocostalis thoracis

548  M.scalenus

549  Nuchal ligament


550  M.spinalis et semispinalis cervicis

551  M.multifidus cervicis

552  M.intertransversarii cervicis

553  M.longus capitis


554  M.longus colli

555  M.sternocephalicus

556

557

558 Fig.8. T1-weighted MRI image at Mid-vertebral level (C7). Muscles are listed dorsal to  
559 ventral, left to right.

560  C7

561  Scapula


562  M.trapezius cervicis

563  M.rhomboideus

564  M.splenius

565  M.serratus ventralis


566  M.semispinalis capitis (Biventer)


567  M.semispinalis capitis (Complexus)


568  M.longissimus capitis

569  M.longissimus cervicis

570  M.longissimus thoracis and M.illiocostalis thoracis

571  M.intertransversarii cervicis

572  Nuchal ligament

573  M.spinalis et semispinalis cervicis

574  M.multifidus cervicis

575  M.longus colli

576

577

578

579

580

581

Fig.9. Sagittal left lateral view of the superficial shoulder girdle muscles (a) 3D image of mapped muscles. (b) Photographic image of the anatomic canine cadaver dissection. 1 - M.cleidocervicalis; 2 – M.trapezius cervicis; 3 –M. sternocephalicus.

Fig.10. Sagittal lateral view from the left of the superficial and deep shoulder girdle muscles and the superficial long neck muscle (a) 3D image of mapped muscles. (b) Photographic image of the anatomic canine cadaver dissection. 1- M.rhomboideus; 2 - M.splenius; 3 - M.serratus ventralis; 4 - M.omotransversarius.